Crystallographic and magnetic transitions in CeVO₃: A neutron diffraction study

A. Muñoz*

Departamento de Física Aplicada, EPS, Universidad Carlos III, Avda. Universidad, 30, Leganés-Madrid, E-28911, Spain

J. A. Alonso, M. T. Casáis, M. J. Martínez-Lope, and J. L. Martínez

Instituto de Ciencia de Materiales de Madrid, CSIC, Cantoblanco, E-28049 Madrid, Spain

M. T. Fernández-Díaz

Institut Laue Langevin, Boîte Postal 156X, Grenoble, F-38042, France

Polycrystalline CeVO₃ has been studied by neutron powder diffraction (NPD), specific heat, and magnetization measurements. CeVO₃ becomes magnetically ordered below $T_N \approx 136$ K and an anomalous-diamagnetism effect is observed below $T_t \approx 124$ K under zero-field-cooling conditions. Simultaneously, a crystallographic transition is observed by NPD at T_t, from the high-temperature orthorhombic structure, space group *Pnma*, to a low-temperature monoclinic structure, space group $P2_1/n$. When cooling the sample across this transition the perovskite distortion evolves from the O type, with $b/(c\sqrt{2}) > 1$, to the O′ type, characterized by $b/(c\sqrt{2}) < 1$, involving a significant increase in the distortion of the VO₆ octahedra. Neutron diffraction measurements revealed that, below T_N, the magnetic ordering is characterized by the propagation vector **k**=0, concerning only the vanadium magnetic moments, which adopt a spin arrangement given by the basis vector $(0,0,G_z)$. Thus, the magnetic moments are antiferromagnetically coupled in the *a-c* plane, and the *a-c* layers couple ferromagnetically along the *b* direction. At around 50 K there is a transition to a different magnetic spin arrangement, also characterized by **k**=0. A ferromagnetic component appears on the V³⁺ cations, which adopt the magnetic structure $(F_x,0,G_z)$; on the other hand, the cerium magnetic moments also become ordered with a spin arrangement given by $(F'_z,0,G'_z)$. At $T=2.6$ K the magnetic moments for the V³⁺ and Ce³⁺ ions are 1.72(4) μ_B and 0.46(3) μ_B, respectively.

I. INTRODUCTION

Rare-earth orthovanadates with the chemical formula RVO₃ form a very interesting system that exhibits outstanding physical properties, such as anomalous diamagnetism and a simultaneous crystallographic-antiferromagnetic transition. The compounds of this system are semiconducting or insulating, although some of them, such as the Mott insulator YVO₃ oxide, can become metallic by carrier doping.

The first crystallographic studies reported in the fifties described RVO₃ from R = Pr to Lu as orthorhombic,[1–3] with $a \approx c \approx \sqrt{2}a_p$ and $b \approx 2a_p$, *Pnma* space group (the long axis parallel to the *b* direction), whereas LaVO₃ was considered to be cubic with $a \approx \sqrt{2}a_p$, being a_p the lattice parameter of the ideal cubic perovskite. A subsequent work carried out on LaVO₃ showed that this compound is also orthorhombic, isostructural with GdFeO₃.[4] A decrease in the orthorhombic unit-cell volume is observed on decreasing the ionic radius of the R³⁺ cation, as expected by the lanthanide contraction effect.

Below the magnetic ordering temperature, with T_N ranging from 137 K for LaVO₃ to 101 K for LuVO₃,[5] the members of the series adopt an antiferromagnetic-canted magnetic structure. Below T_N only the V³⁺ ions contribute to the long distance ordering, which exhibit a magnetic moment value in good agreement with the $3d^2$ electronic configuration $S=1$. From La to Dy (except for Sm, Eu, and Gd whose magnetic structure has not been determined due to the strong

neutrons absorption) the magnetic structure of the rare-earth orthovanadates is **G** type, whereas from Ho to Lu and for Y the structure is defined by the basis vector **A** (in both cases within the *Pnma* setting). In the ordered region, a rearrangement of the magnetic moments has been reported for some of the rare-earth orthovanadates. A reorientation of the moments has been observed in PrVO₃ and NdVO₃.[5] In YVO₃, the magnetic structure was described to change from A_zF_y to G_xF_z below $T_s = 77$ K (*Pnma* setting), although a subsequent study established that the structure below T_s is A_zF_y, and it is defined by G_xF_z for $T_s < T < T_N$.[6] The neutron diffraction study also showed a small ferromagnetic component, suggesting the presence of a weak ferromagnetism effect.

The magnetic properties of the rare-earth orthovanadates have been well studied;[5,7–19] the most singular feature is the presence of the anomalous diamagnetism effect. In LaVO₃, below a characteristic transition temperature T_t, some degrees below T_N, a sharp drop in the field cooled (FC) susceptibility is observed, reaching a negative value. A similar behavior takes place in the zero field cooled (ZFC) susceptibility in CeVO₃. This anomalous diamagnetism is associated with a reversal of the weak ferromagnetic component caused by a cooperative first-order magnetostrictive distortion[16,20] at T_t. Although in polycrystalline samples of YVO₃ the anomalous diamagnetism phenomenon is not observed, in single crystals, a reversal of the ferromagnetic component with respect to the applied magnetic field is displayed in the temperature interval $77 < T < 95$ K.[19] The magnetostrictive distortion is related to a crystallographic transi-

tion that occurs a few degrees below T_N. The orthorhombic magnetic structure becomes monoclinic, as it has been described for LaVO$_3$,[4] YVO$_3$,[21] and for YbVO$_3$.[15] The crystallographic transition is clearly observed in the specific-heat measurements of these three rare-earth orthovanadates.[22–25] On the other hand, for the rare-earth orthovanadates formed with the lighter rare-earth atoms, the crystallographic transition is accompanied by a change in the type of orthorhombic distortion. At room temperature the structure is O orthorhombic with $b/(\sqrt{2}c)>1$, whereas the distortion becomes O', $b/(\sqrt{2}c)<1$, (*Pnma* setting in both cases), below the crystallographic transition.

A detailed study of the subtle structural changes experienced by RVO$_3$ perovskites for the lighter terms of the series is lacking. In this work we have followed the structural transition experienced by CeVO$_3$ from neutron diffraction. We also present accurate structural data at RT and 2 K from high resolution neutron diffraction data. On the other hand, a magnetic structure and its thermal evolution below T_N has also been investigated. The characterization of the sample has been completed with susceptibility and specific heat measurements.

II. EXPERIMENTAL

CeVO$_3$ perovskite was prepared in polycrystalline form by soft-chemistry procedures. Stoichiometric amounts of analytical grade Ce(NO$_3$)$_3 \cdot$6H$_2$O and NH$_4$VO$_3$ were dissolved in citric acid; the citrate+nitrate solutions were slowly evaporated, leading to an organic resin containing an homogeneous distribution of the involved cations. This resin was first dried at 120 °C and then slowly decomposed at temperatures up to 800 °C in air, for 2 h. This treatment gave rise to CeVO$_4$, conformed as a highly reactive precursor material. The final reduction process was performed at 1160 °C for 12 h in a H$_2$/N$_2$ (15%/85%) flow.

The susceptibility measurements were performed in a commercial SQUID magnetometer. The dc susceptibility curve was obtained both under zero-field cooling (ZFC) and field-cooling (FC) conditions, and in both cases under a 50 Oe magnetic field and for temperatures ranging from 1.8 to 300 K. The specific heat measurements were carried out in a semiadabatic He calorimeter with a ^{3}He insert, using the heat-pulsed method for temperatures going from 0.35 to 160 K under a zero and 10, 30, 60, and 90 kOe magnetic field.

High-resolution neutron powder diffraction (NPD) patterns were collected at room temperature and at 2 K at the D2B diffractometer of the Institut Laue-Langevin in Grenoble (France), with a wavelength of 1.59 Å. A set of NPD patterns were also dynamically acquired between 2.6 and 300.5 K at the high-flux D20 diffractometer, with a wavelength $\lambda=2.40$ Å. The data were acquired in the heating run [1 K min (Ref. 1)], being the counting time of 5 min per diagram. The sequential NPD patterns were used to study the magnetic structure and its thermal evolution, as well as to follow the subtle changes in the crystallographic structure. The neutron diffraction data were analyzed by the Rietveld method,[26] using the FULLPROF program[27] for the refinement of the crystallographic and the magnetic structures. In the
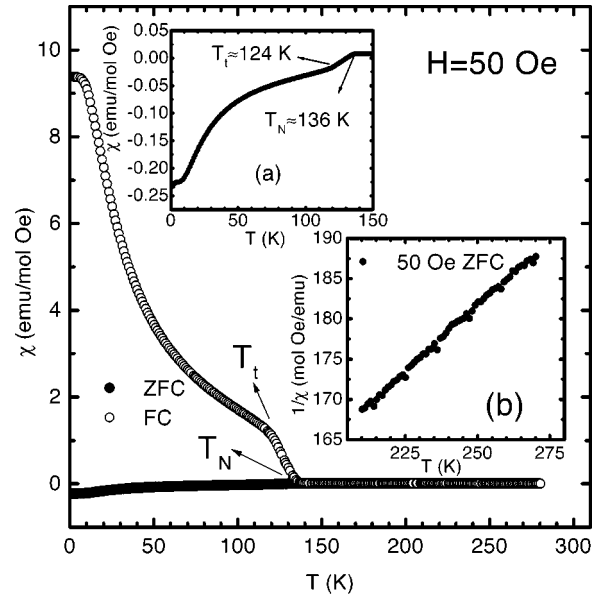

FIG. 1. Thermal evolution of the dc susceptibility measured under a 50 Oe magnetic field, in zero field-cooling (ZFC) and field-cooling (FC) conditions. Inset: (a) Thermal evolution of the susceptibility (ZFC) below 150 K; (b) Inverse of the susceptibility in the temperature range $210<T<270$ K (ZFC).

fitting, the profile was simulated by a pseudo-Voigt function and the background was adjusted with a fifth-degree polynomial function.

III. RESULTS FROM MAGNETIC AND SPECIFIC HEAT MEASUREMENTS

A. Magnetic measurements

The thermal evolution of the zero field cooling (ZFC) and the field cooling (FC) susceptibility curves obtained under a 50 Oe magnetic field are shown in Fig. 1. The ZFC and the FC curves coincide at high temperature and split out below 136 K, indicating the appearance of a magnetic order with $T_N\approx136$ K. On decreasing temperature below T_N a change in the slope of the susceptibility of the FC curve occurs at around $T_t\approx124$ K. Simultaneously, the ZFC susceptibility, that decreases on decreasing the temperature below T_N, becomes negative below T_t [see inset (a) in Fig. 1], what implies a reversal of the magnetization with respect to the applied magnetic field. This behavior of the magnetic susceptibility is in good agreement with previous experimental measurements presented by Nguyen *et al.*[17] The ZFC magnetization decreases monotonically with temperature, experiencing a more pronounced variation below 50 K. Below 7 K the susceptibility tends to saturation. In the paramagnetic region, the inverse of the dc susceptibility does not present a linear behavior [inset (b) in Fig. 1], therefore, in the temperature interval $210<T<270$ K, and in a first approximation, the dc susceptibility is fitted according to the Curie-Weiss law $\chi=C/(T-\Theta_P)+\chi_0$. C is the Curie constant, Θ_P is the Weiss temperature, and χ_0 is the temperature independent term. The fitting gives $C=2.04(2)$ emu K/mol, a paramagnetic temperature $\Theta_P=-206(3)$ K and $\chi_0=0.0010(3)$
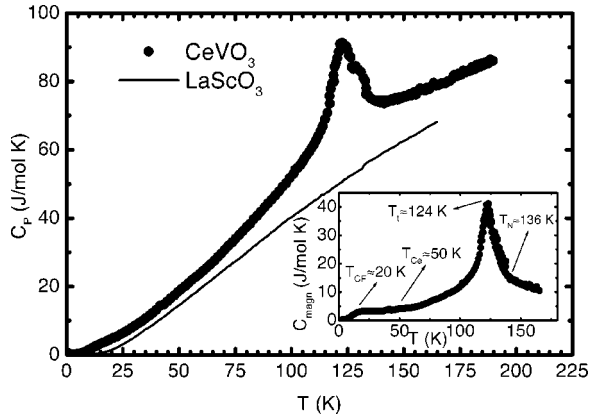
FIG. 2. Temperature dependence of the specific heat without magnetic field. Inset: Magnetic contribution to the specific heat.

FIG. 3. Temperature dependence of the specific heat under different applied magnetic fields. Inset: Enhancement of C_p versus T/T_{max}.

emu/mol K. The χ_0 term is mainly due to the Van Vleck–type contribution caused by the influence of the crystal field on the Ce^{3+} ions. The Curie constant implies an effective magnetic moment $\mu_{eff} = 4.0(1)$ μ_B. The system is composed of two different sublattices of spins V^{3+} and Ce^{3+} and, in a first order approximation, by considering them as two non-interacting systems of isolated spins, the effective magnetic moment can be estimated through the relationship[28,29] $\mu_{eff} = \sqrt{[\mu_{eff}(V^{3+})]^2 + [\mu_{eff}(Ce^{3+})]^2}$. On assuming that both sublattices of spins are in the ground state, with $\mu_{eff}(V^{3+}) = 2.83$ μ_B (spin only, $S=1$) and $\mu_{eff}(Ce^{3+}) = 2.54\mu_B$ ($^2F_{5/2}$), an effective magnetic moment value of 3.80 μ_B is obtained, which is in good agreement with the experimental value.

B. Specific heat measurements

The thermal variation of the specific heat C_P under a zero magnetic field is represented in Fig. 2. On decreasing the temperature, a sharp anomaly is observed, which is formed by the convolution of two peaks. The high temperature shoulder corresponds to the onset of magnetic ordering with $T_N \approx 136$ K, whereas the second one, with a maximum at around $T_t \approx 124$ K, corresponds to a crystallographic transition, as it will be shown from the neutron diffraction data. Both anomalies are in good agreement with the results of the susceptibility measurements. On the other hand, as it is clearly shown in Fig. 3, in the lowest temperature region the specific heat curve exhibits the characteristic behavior given by a Schottky-like anomaly. In order to estimate the magnetic contribution to the specific heat curve under a zero magnetic field, the contribution due to the lattice vibrations must be evaluated. The specific heat of the nonmagnetic and isostructural compound $LaScO_3$, measured in the temperature interval $1.8 < T < 164.8$ K is shown in Fig. 2. On assuming that the lattice contribution to the specific heat in $CeVO_3$ is the same as in $LaScO_3$, the magnetic contribution can be estimated by a simple subtraction of both curves (inset in Fig. 2) with the corresponding weigh factors. In the curve corresponding to the magnetic contribution of the specific heat (inset in Fig. 2), in addition to the anomalies at T_N and T_t, another two anomalies are observed, one at around T_{Ce}
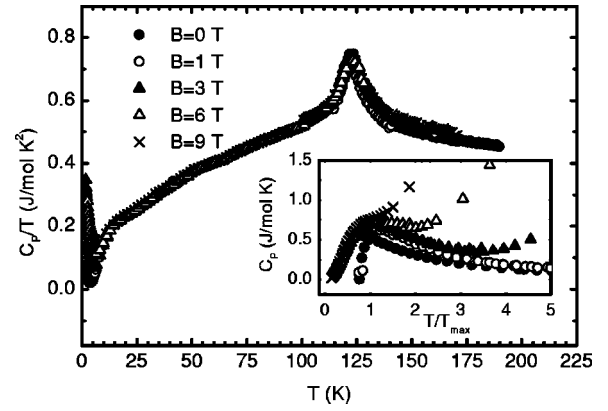
≈ 50 K and another one at around $T_{CF} \approx 20$ K. As it will be shown in the magnetic structure resolution, the transition at T_{Ce} corresponds to the ordering of the Ce^{3+} sublattice. As regarding the transition at T_{CF}, as it will be pointed out later on, it is due to a transition between the two lowest doublets of the three Krammers doublets associated with the Ce^{3+} ion. The entropy change that takes place in the temperature range $3.1 < T < 150$ K and that has been estimated with the expression $\int (C_{magn}/T)dT$, is $\Delta S = 18.26$ J/mol K.

The specific heat curves measured under different magnetic fields are represented as C_P/T versus T in Fig. 3. According to Fig. 3, there are no significant differences between the different curves, except in the Schottky anomaly. This anomaly is associated with the Ce^{3+} ions. The ground state of the Ce^{3+} ion is $^2F_{5/2}$ with a $J = 5/2$ multiplet, that, for an odd number of electrons, splits into three Kramers doublets, due to the crystal field effect. The ground state is a doublet and as the Schottky anomaly appears at very low temperature, it can be assumed that only this doublet is involved in the Schottky effect. The two levels of the doublet are separated either because of the internal magnetic field originated both for the Ce-Ce and Ce-V exchange interactions or because the presence of an external magnetic field. The specific heat for the two level Schottky specific heat[30] is

$$C_{Schottky} = pR \left(\frac{\Delta}{T}\right)^2 \frac{g_0}{g_1} \frac{e^{\Delta/T}}{\left[1 + \left(\frac{g_0}{g_1}\right)e^{\Delta/T}\right]^2} \quad (1)$$

where p is the number of atoms in a molecule, R is the gas constant, Δ is the energy separation between the lowest a first excited level, and g_0 and g_1 are, respectively, the degeneracy of both energy levels. The maximum value of the specific heat happens at T_{max}

$$\frac{g_0}{g_1} e^{\Delta/T_{max}} = \frac{(\Delta/T_{max}) + 2}{(\Delta/T_{max}) - 2} \quad (2)$$

and at T_{max} the maximum value of the specific heat is

TABLE I. Analysis of the Schottky specific heat anomaly.

B (T)	T_m(K)	Δ(K)	ΔS(J/molK)
0	0.43	0.88	0.57
1	0.65	1.36	0.74
3	1.46	3.04	a
6	2.70	5.62	1.19
9	4.40	9.20	1.00

aThe temperature range is not enough for a correct evaluation of the entropy

$$C_{\text{Schottky}}(\text{max}) = \frac{pR}{4}\left[\left(\frac{\Delta}{T_{\text{max}}}\right)^2 - 4\right]. \tag{3}$$

For the Ce^{3+} ions, $p=1$ and $(g_0/g_1)=1$, so on considering the experimental T_{max} and C_{Schottky} (max), the energy split between both levels has been determined for the different specific heat curves measured under different magnetic fields (see Table I). The entropy content for the specific heat, calculated through the expression $\int (C_p/T)dT$, is included in Table I. The theoretical entropy content of the Schottky curve can be evaluated if it is taken into consideration that there are two levels, hence $\Delta S = R\ln(2) = 5.76$ J/mol. The experimental values are below the calculated one.

For a better comparison, the Schottky curves are plotted as C_P versus T/T_{max} (inset of Fig. 3). For $T < T_{\text{max}}$, the specific heat decreases with temperature and it tends towards zero; however, for $T > T_{\text{max}}$, C_P decreases on increasing temperature only under a low magnetic field ($B=0$, 1 T); for $B=3$, 6, and 9 T, C_P tends to increase above a critical temperature that for higher magnetic field is closer to the T_{max}. This behavior can be accounted for, on considering the two level Schottky specific heat. For the low magnetic field curves both the T_{max} and the energy split of both levels Δ is small, so the Schottky behavior dominates. For $T < T_{\text{max}}$ the ground state tends to be the most populated in such a way that, on decreasing temperature, the thermal energy is not enough to populate the excited level: therefore the specific heat tends to zero. For $T > T_{\text{max}}$, on increasing temperature, both levels tend to be equally populated and the specific heat tends to decrease. For high magnetic fields, T_{max} and Δ are much higher, hence for $T > T_{\text{max}}$ the contributions of the lattice and magnetic excitations to the specific heat increase and hide the Schottky behavior.

Under a zero magnetic field, the thermal evolution of the magnetic contribution (inset in Fig. 2) shows a Schottky-type behavior above 4 K with a maximum at around $T_{\text{CF}} \approx 20$ K. This can be associated with a transition to the first excited Krammers doublet, which could start to participate in this temperature range. However, this anomaly does not vary on applying a magnetic field, in contrast with the variation found in the Schottky anomaly at much lower temperatures. This feature can be associated with the fact that this anomaly is meanly due to the energy separation between the center of gravity of both doublets, which is only determined by the crystal field. This mechanism would be possible if the energy separation between the doublets is much greater than the splitting of the excited Krammers doublet. By considering a two level scenario, and from the values observed in the C_{magn} curve (inset Fig. 2), the center of gravity of both doublets would be separated by a $\Delta \approx 47$ K energy.

IV. NEUTRON DIFFRACTION MEASUREMENTS

A. Crystallographic structure

The refinement of the crystal structure at room temperature was carried out from a high resolution neutron diffraction pattern acquired with a wavelength $\lambda = 1.59$ Å. The Bragg reflections of the pattern could be indexed by considering an orthorhombic unit cell, space group *Pnma*. This structure contains a single position for V atoms, and two independent positions for oxygens O1 ($4c$) and O2 ($8d$). The lattice parameter values obtained in the fitting are presented in Table II. The atomic positions and some selected atomic distances are listed in Tables III and IV, respectively. The good agreement between experimental and calculated NDP profiles after the Rietveld refinement is displayed in Fig. 4(a). No extra peaks were detected in the NPD pattern that could indicate the presence of impurities in the sample.

A set of sequential NPD patterns collected between 2.6 and 300.5 K with a wavelength $\lambda = 2.40$ Å, were considered to analyze the crystal structure evolution across the anomaly observed around T_N. On decreasing the temperature below T_N some changes in some of the Bragg reflections are symptomatic of a crystallographic phase transition, happening at relatively high angles that exclude the presence of a magnetic contribution. This is illustrated in Fig. 5, where the thermal variation of the nuclear peak located between $2\Theta = 60.5°$ and $2\Theta = 63.7°$ is given. In the space group *Pnma*, this peak is formed by the reflections (211), (112), and (031); some degrees below T_N the peak spreads out, indicating the appearance of new Bragg reflections that correspond to a symmetry lowering. The low-temperature crystal structure can be defined in the monoclinic $P2_1/n$ space group; in particular, in the angular range $60.5 < 2\Theta < 63.7$ the new reflections (21-1), (11-2), and (130) explain the broadening of the diffraction peak shown in Fig. 5.

The refinement of the monoclinic structure was performed from a high resolution NPD pattern collected at 2 K with $\lambda = 1.59$ Å. The pattern was fitted with the $P2_1/n(C_{2h}^5)$ monoclinic space group (the twofold axis parallel to a), with unit-

TABLE II. Lattice parameter for CeVO₃.

	Space group	a(Å)	b(Å)	c(Å)	α(°)	Vol(Å³)
RT	*Pnma*	5.5376(2)	7.7864(3)	5.5039(2)	90	237.32(2)
$T=2$ K	$P2_1/n$ 1 1	5.5730(4)	7.7038(5)	5.5148(3)	89.954(9)	236.77(3)

TABLE III. Structural parameters obtained from the Rietveld refinement of the high resolution NPD pattern with $\lambda = 1.59$ Å.

Atoms	Positions	RT($Pnma$)	$T=2K(P2_1/n\ 1\ 1)$
	x	0.0374(8)	0.0394(10)
Ce	y	0.25	0.252(2)
	z	0.9907(14)	0.9905(10)
	$B(\text{Å}^2)$	0.53(7)	0.47(9)
	x	0.50	0.50
V1	y	0.00	0.00
	z	0.00	0.00
	$B(\text{Å}^2)$	0.4	0.20
	x		0.00
V2	y		0.00
	z		0.50
	$B(\text{Å}^2)$		0.20
	x	0.4844(7)	0.4870(7)
O1	y	0.25	0.2465(14)
	z	0.0772(8)	0.0768(8)
	$B(\text{Å}^2)$	0.76(6)	0.34(5)
	x	0.2886(5)	0.2756(11)
O2	y	0.0412(3)	0.00363(8)
	z	0.7117(5)	0.7103(15)
	$B(\text{Å}^2)$	0.68(4)	0.34(5)
	x		0.1977(13)
O3	y		0.9520(10)
	z		0.2103(15)
	$B(\text{Å}^2)$		0.34(5)
	R_p	4.2%	5.0%
Discrep.	R_{wp}	5.2%	6.5%
factors	R_{Bragg}	7.1%	9.4%
	χ^2	1.1	1.8

TABLE IV. Selected interatomic distances (in Å). V1 is at (1/2,0,0) and V2 at (0,0,1/2).

	RT($Pnma$)		$T=2\ K(P2_1/n\ 1\ 1)$
Ce-O1	2.396(9)		2.404(7)
Ce-O1	2.520(6)		2.539(7)
Ce-O2(×2)	2.405(5)		2.461(11)
Ce-O2(×2)	2.634(6)		2.622(11)
Ce-O2(×2)	2.748(5)		2.711(13)
Ce-O3			2.331(12)
Ce-O3			2.630(12)
Ce-O3			2.751(13)
$\langle$Ce-$O\rangle$	2.561(2)		2.556(11)
V-O1(×2)	1.9943(10)	V1-O1(×2)	1.947(10)
V-O2(×2)	1.998(3)	V1-O2(×2)	2.048(7)
V-O2'(×2)	2.004(3)	V1-O3(×2)	2.078(7)
		V2-O1(×2)	1.999(10)
		V2-O2(×2)	1.945(7)
		V2-O3(×2)	1.976(8)
$\langle$V-O$\rangle$	1.9995(5)		1.999(8)
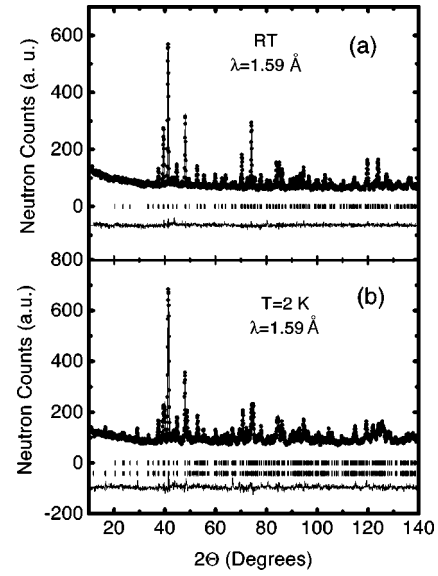
FIG. 4. Observed (solid circles), calculated (solid line), and difference (bottom line) NPD patterns. (a) NPD pattern at room temperature and (b) NPD pattern at $T=2$ K. The first row of tic marks correspond to the Bragg reflections of $CeVO_3$, in (b) the second row corresponds to the magnetic peaks.

cell parameters related to a_p (ideal cubic perovskite, $a_p \approx 3.8$Å) as $a \approx \sqrt{2}a_p$, $b \approx 2a_p$, $c \approx \sqrt{2}a_p$. In the $P2_1/n$ phase there are two crystallographically independent V positions (V1 and V2), as well as three kinds of nonequivalent oxygen atoms (O1, O2, and O3) all in general positions. V1O$_6$ and V2O$_6$ octahedra alternate along the three directions of the structure, in such a way that each V1O$_6$ octahedron is linked to six V2O$_6$ octahedra, and vice-versa. The a parameter, characterizing the low-temperature monoclinic distortion [89.954(9)$^\circ$ at 2 K], slightly deviates from 90°, indicating a strongly pseudo-orthorhombic metric, which enforces the use of very high resolution tools. The quality of the fit is shown in Fig. 4(b) and the characteristic parameters after the refinement are presented in Tables II, III, and IV.
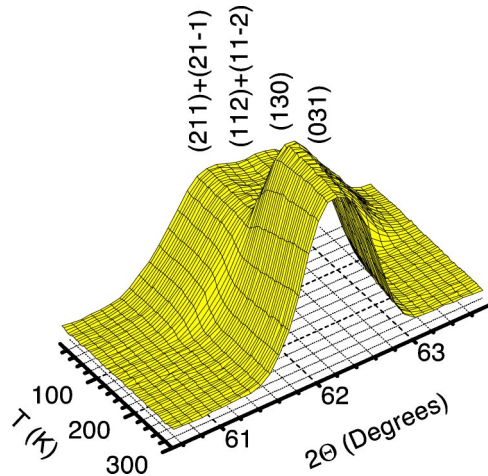
FIG. 5. Thermal evolution of the NPD patterns in the temperature range $2.6 < T < 300.5$ K and for $60.5 < 2\Theta < 63.7$ collected in D20 in the heating run with $\lambda = 2.40$ Å.
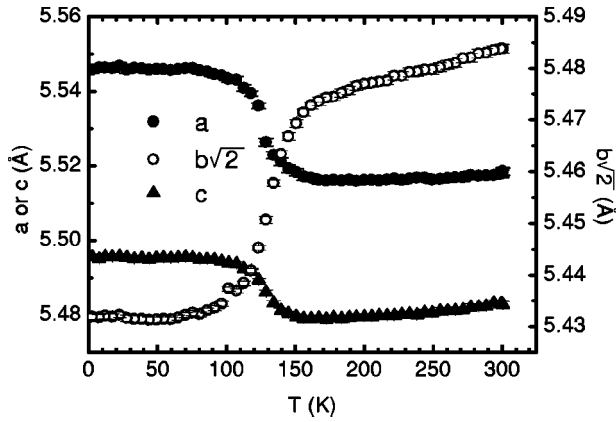
FIG. 6. Thermal variation of the lattice parameters. For $50 < T < 300.5$ K *Pnma* space group and for $2.6 < T < 50$ K $P2_1/n$ space group.

FIG. 8. Thermal variation of the V-O atomic distances. In the calculations it has been considered that the crystallographic structure is orthorhombic, *Pnma* space group.

The analysis of the thermal evolution of the crystallographic structure has been carried out by sequentially refining the NPD patterns collected in the temperature range 2.6–300.5 K. The thermal variation of the lattice parameters is presented in Fig. 6. An important change in the lattice parameters takes place between 100 and 150 K. These variations also originate important changes in the unit-cell volume, as it can be seen in Fig. 7. The volume, that uniformly decreases on cooling from room temperature, undergoes a steeper decrease at around $T_N \approx 136$ K, and then experiences an abrupt increase at around $T_t \approx 127$ K. On the other hand, there is also a change in the type of the orthorhombic distortion in CeVO$_3$, defined as a function of the ratio $b/(c\sqrt{2})$. Above the transition, $b/(c\sqrt{2}) > 1$ (O-type), which transforms to $b/(c\sqrt{2}) < 1$ (O′-type) below the transition; in both cases the *Pnma* setting is used. Although the transformation starts to be noticed at around 220 K, the ratio $b/(c\sqrt{2})$ suffers the most important decrease between 100 and 150 K.

The thermal evolution of the atomic distances, in particular the V-O bond lengths, has also been studied. Below T_t, the fitting of the NPD patterns has also been carried out in
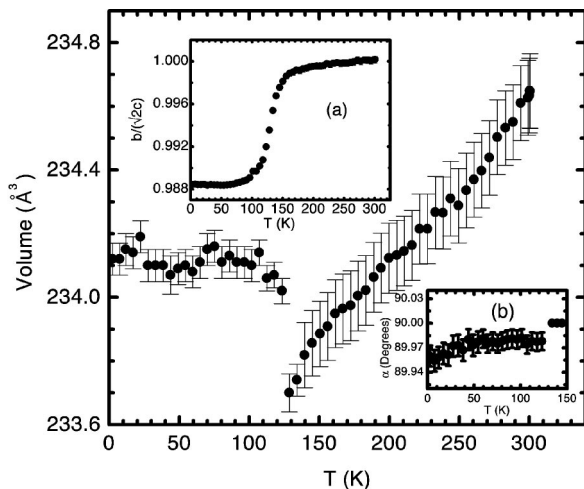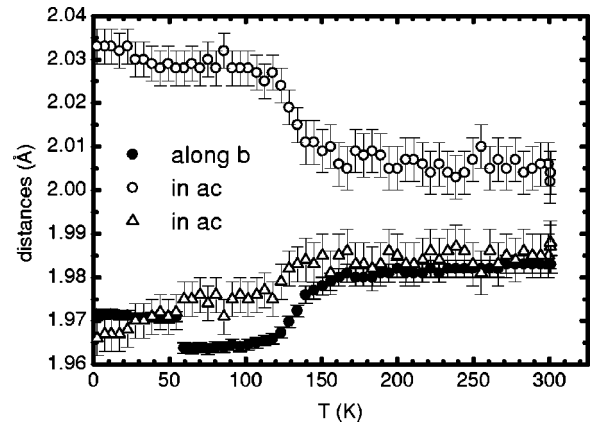

FIG. 7. Thermal evolution of the unit cell volume. Inset: (a) thermal variation $b/(\sqrt{2})$. (b) Thermal evolution for α.

the *Pnma* space group (the monoclinic α angle is very close to 90°). Although the structure is monoclinic in this temperature range the resolution of the NPD patterns collected with $\lambda = 2.42$ Å is not high enough to enable a full refinement in the $P2_1/n$ space group, which would give rise to large errors in the V-O distances. The thermal variation of the V-O distances determined in this way is presented in Fig. 8. The short equatorial V-O2 distance in the *ac* plane and the V-O1 distance along b are similar at high temperature, but they split out below 150 K. The changes in the V-O distances take place between 120 and 150 K. Let us point out that the axial V-O1 distance along b undergoes an abrupt increase at around 50 K. The short V-O2 equatorial distance also suffers a change at around this temperature. We will show later that this structural change is correlated to a magnetic transition that takes place at around 50 K.

B. Magnetic structure resolution

Upon cooling below 140 K, the (100)+(001) and the (120)+(021) Bragg reflections, that are forbidden by the *Pnma* space group, start to be observed (see Fig. 9), indicating the appearance of a magnetic ordering below T_N, in good agreement with the magnetic measurements. The magnetic structure is defined by the propagation vector **k**=0, and only those magnetic reflections with $k = 2n$ and $h + l = 2n + 1$ are observed. As temperature decreases, the intensity of the magnetic peaks increases until nearly achieving saturation, but at around 50 K some new changes are observed in the NPD patterns. As shown in Fig. 9, the intensity of the observed magnetic (100)+(001) reflections decrease below this temperature, and in another case, such as the (120)+(021)+(02-1) reflections, increase with a steeper slope (see Fig. 9). On the other hand, new reflections appear, as shown in Fig. 10 for the (10-1)+(101)+(020) and (200)+(002)+(121)+(12-1) reflections. This reveals the establishment of a new magnetic arrangement. In the new magnetic structure, the magnetic unit cell also coincides with the chemical one (**k**=0); now the observed magnetic reflections are those with $k = 2n$.
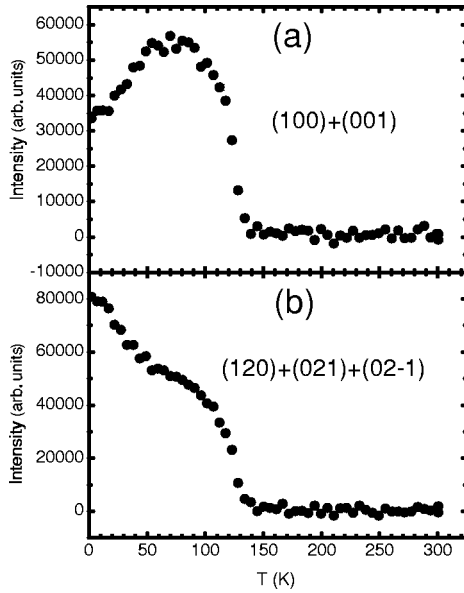
FIG. 9. Thermal variation of the magnetic peaks $(100)+(001)$ and $(120)+(021)+(02\text{-}1)$.

In the resolution of the magnetic structure, we have taken into consideration those solutions that are compatible with the symmetry of the space group and that are presented in Tables V and VI. For the V atoms, we have considered those solutions with equal moments for both vanadium sites V1 and V2. Let us point out that in the temperature range $124 < T < 136$ K, the structure is orthorhombic (space group *Pnma*) and there is only a site for the V atoms; in this case, all the solutions deduced by the group theory analysis imply the same magnetic moment for all the vanadium atoms.[31]

In the temperature range $50 < T < 136$ K, and after checking all the different solutions, the best agreement with the experimental data is obtained if only the vanadium magnetic
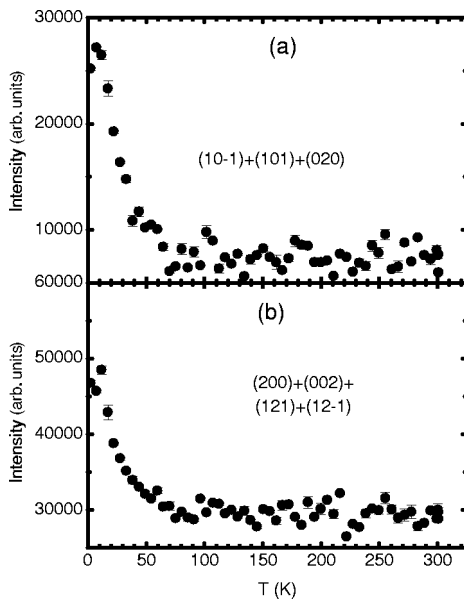

FIG. 10. Thermal variation of the magnetic peaks $(10\text{-}1)+(101)$ $+(020)$ and $(200)+(002)+(121)+(12\text{-}1)$.

TABLE V. Basic vectors for the V^{3+} ions, which has been taken from Ref. 15.

	V1		V2		
	2(1/2,0,0)	3(0,1/2,1/2)	1(0,0,1/2)	4(1/2,1/2,0)	Eq. mom.
Γ_1	$\begin{bmatrix}1\\1\\1\end{bmatrix}$	$\begin{bmatrix}1\\\bar{1}\\\bar{1}\end{bmatrix}$	$\begin{bmatrix}1\\\bar{1}\\\bar{1}\end{bmatrix}$	$\begin{bmatrix}1\\\bar{1}\\\bar{1}\end{bmatrix}$	(F_x,A_x) (C_y,G_y) (C_z,G_z)
Γ_2	$\begin{bmatrix}1\\1\\1\end{bmatrix}$	$\begin{bmatrix}\bar{1}\\1\\1\end{bmatrix}$	$\begin{bmatrix}1\\1\\1\end{bmatrix}$	$\begin{bmatrix}\bar{1}\\1\\1\end{bmatrix}$	(C_x,G_x) (F_y,A_y) (F_z,A_z)

moments become ordered and the spin arrangement is given by the basis vector $(0,0,G_z)$.[32] The G_z basis vector implies that the coupling among the magnetic moments is $m_{1z} = -m_{2z} = m_{3z} = -m_{4z}$; the notation for the position of the V atoms is given in Table V. For this coupling, only the reflections with $k = 2n$ and $h + l = 2n + 1$ are allowed. The good agreement between the observed and calculated NPD patterns at $T = 64.8$ K is presented in Fig. 11(a). As it is indicated in Table VII, at $T = 64.8$ K the refined magnetic moment for the ordered vanadium atoms is $\mu = 1.31(3)$ μ_B.

In the temperature range $T < 50$ K, the fitting of the experimental data is only acceptable if we assume that both V^{3+} and Ce^{3+} ions participate in the magnetic ordering. The spin arrangement is given by $(F_x,0,G_z)$ and $(F'_x,0,G'_z)$ for the V^{3+} and Ce^{3+} ions, respectively. The ferromagnetic component for the Ce^{3+} ions is negligible, for instance at $T = 2.6$ K the ferromagnetic component value is $0.11(5)$ μ_B. In contrast, at the same temperature, for the V^{3+} ions the ferromagnetic component value is $0.87(6)$ μ_B. The results of the fitting at $T = 2.6$ K are listed in Table VII and the good agreement between the calculated and observed NPD patterns can be seen in Fig. 11(b). The thermal evolution of the magnetic moments in all the temperature range is shown in Fig. 12. The magnetic structure in both temperature ranges is represented in Fig. 13.

V. DISCUSSION

The magnetization and specific heat measurements have confirmed that $CeVO_3$ becomes magnetically ordered below

TABLE VI. Basic vectors for the Ce^{3+} ions. The notation for the posicions are $5(x,y,z),6(\bar{x}+1/2,y+1/2,\bar{z}+1/2),7(\bar{x},\bar{y},\bar{z})$ and $8(x+1/2,\bar{y}+1/2,\bar{z}+1/2)$.

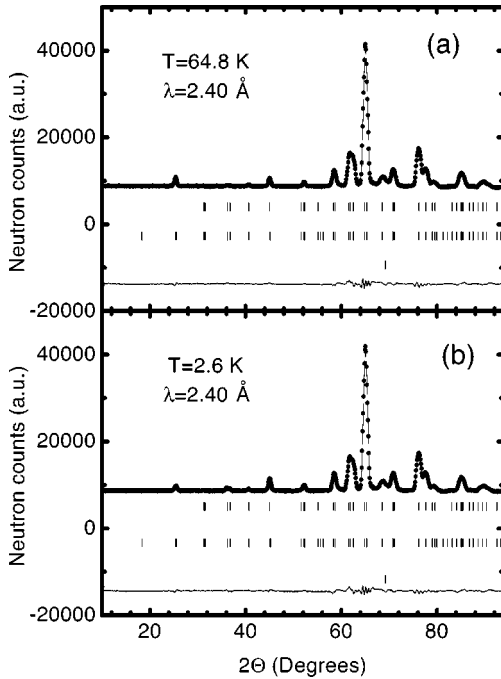|	Ce5	Ce6	Ce7	Ce8	
Γ_1	$[111]$	$[1\bar{1}\bar{1}]$	$[111]$	$[1\bar{1}\bar{1}]$	(F'_x,G'_y,G'_z)
Γ_2	$[111]$	$[\bar{1}11]$	$[\bar{1}\bar{1}\bar{1}]$	$[1\bar{1}\bar{1}]$	(A'_x,C'_y,C'_z)
Γ_3	$[111]$	$[\bar{1}11]$	$[111]$	$[\bar{1}11]$	(G'_x,F'_y,F'_z)
Γ_4	$[111]$	$[1\bar{1}\bar{1}]$	$[\bar{1}\bar{1}\bar{1}]$	$[\bar{1}11]$	(C'_x,A'_y,A'_z)

FIG. 11. Observed (solid circles), calculated (solid line), and difference (bottom line) NPD patterns. (a) For $T=64.8$ K and (b) for $T=2.6$ K. The first row of tic marks correspond to the Bragg reflections of CeVO$_3$, the second row to the magnetic peaks and the third row to the vanadium sample holder.

$T_N \approx 136$ K. Neutron diffraction measurements have shown that immediately below T_N, only the vanadium moments participate in the magnetic ordering, adopting a spin arrangement given by the basis vector $(0,0,G_z)$. On the other hand, at $T_t \approx 124$ K the sample undergoes a crystallographic transition from a high-temperature orthorhombic structure, space group *Pnma*, to a low-temperature monoclinic structure, space group $P2_1/n$. The anomaly observed in the specific heat measurements at around 50 K corresponds to the appearance of a ferromagnetic component along the *a* direction on the vanadium atoms, and to the simultaneous ordering of the Ce atoms. The spin arrangement for the Ce atoms is given by $(F'_x, 0, G'_z)$; this basis vector belongs to the same irreducible representation than that defining the magnetic structure for the V atoms.
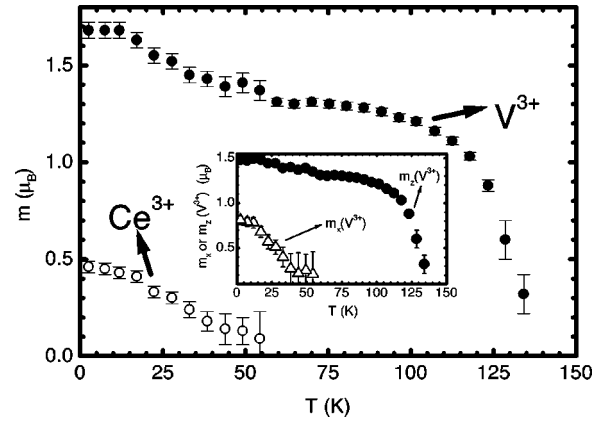

FIG. 12. Thermal evolution of the magnetic moments for the V^{3+} and Ce^{3+} ions. Inset: Thermal evolution of the individual components for the V^{3+} sublattice.

The ordering of the Ce^{3+} ions is clearly observed in the NPD data, since important changes in the thermal evolution of the magnetic reflections appear at around 50 K, which cannot be explained by a change in the arrangement of the magnetic moments of the V^{3+} ions. At low temperature, the magnetic moments of the V^{3+} and Ce^{3+} ions, and also, the ferromagnetic component in the V^{3+} ions seem to attain saturation. The saturation of the ferromagnetic component can account for the saturation observed in the FC susceptibility below 7 K.

It is worthwhile to compare the entropy change that appears in the specific heat below T_N, for instance, for the zero magnetic field curve, with the theoretical one. For the V^{3+} cations, the expected entropy change for spin only $S=1$ is $\Delta S_1 = R\ln(2S+1) = 9.13$ J/mol K; the ground state of the Ce^{3+} cations is $^2F_{5/2}$ with a $J=5/2$ multiplet, what would imply an entropy change $\Delta S = R\ln(6) = 14.90$ J/mol K. So, the total expected entropy change is 24.03 J/mol K. The total change in the entropy observed experimentally below 150 K, if the entropy change in the Schottky anomaly is included, is 19.83 J/mol K. This value is slightly below the expected one. The Ce^{3+} ions order at around $T_{Ce} = 50$ K, which is a relatively high temperature. The ordering can be due either to the Ce-Ce exchange interactions or to the Ce-V interactions, but on considering that at $T=50$ K the ordering in the V sublattice is well established, and as the ordering of the Ce sublattice is given by the basis vectors of the same irreducible

TABLE VII. Results from the magnetic structure determination. In the refinement, it has only be considered the angular range $10 < 2\Theta < 94°$.

	$T=64.8$ K		$T=2.6$ K	
	V^{3+}	Ce^{3+}	V^{3+}	Ce^{3+}
Solution	$(0,0,G_z)$		$(F_x, 0, G_z)$	$(F'_x, 0, G'_z)$
μ_B	$[0,0,1.31(3)]$		$[0.87(6),0,1.49(3)]$	$[-0.11(5),0,-0.45(3)]$
$\lvert m \rvert (\mu_B)$	1.31(3)		1.72(4)	0.46(3)
Discrep.	R_B(nuclear)$=4.7\%$		R_B(nuclear)$=6.9\%$	
Factors	R_B(magnet.)$=6.5\%$		R_B(magnet.)$=10.5\%$	
	$\chi^2 = 2.8$		$\chi^2 = 3.1$	
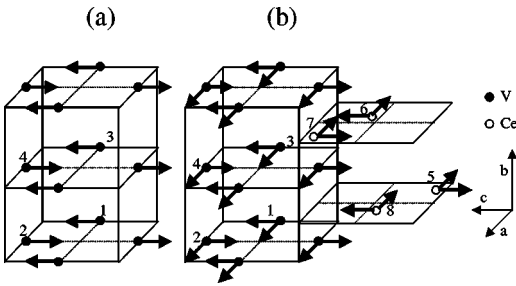
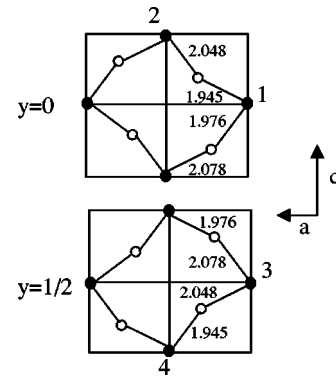FIG. 13. A view of the magnetic structure of $CeVO_3$ (a) for $50 < T < 136$ K and (b) for $T < 50$ K.

FIG. 14. Schematic representation of the V-O bonds (V atoms are the dark circles), displaying the alternation of short and long bonds that suggests an orbital ordering effect (see text). Distances in Å.

representation, it can be assumed that the ordering is mainly caused by the Ce-V exchange interaction. This interaction would originate a molecular field at the Ce positions, that would split the ground Kramers doublet into two levels, which would cause the Schottky anomaly observed in the specific heat. If μ is the effective magnetic moment of the Ce^{3+} ions in the ground state, the effective molecular field can be estimated from the energy separation between the two levels of the doublet determined from the Schottky anomaly, since $\Delta(0) = 2\mu B_{mf}$. In the presence of an external magnetic field it is verified that $\Delta(B) = 2\mu(B + B_{mf})$. From the data obtained at $B = 0$ T and $B = 1$ T an effective magnetic moment $\mu = 0.36$ μ_B and $B_{mf} = 1.8$ T is obtained. This effective magnetic moment is very close to the magnetic moment obtained from the neutron diffraction measurements at $T = 2.6$ K, $\mu = 0.46(3)\mu_B$. By assuming that the molecular field does not change with the magnetic field, it is possible to estimate the effective magnetic moment for the other curves by taking into consideration the splitting of the two levels. The different effective magnetic moments for $B = 3, 6$, and 9 T are, respectively, $\mu = 0.47, 0.53$, and $0.63\mu_B$. These values are coherent with the magnetic moment obtained in the neutron diffraction measurements.

The anomalous diamagnetism observed in the RVO_3 compounds below T_t has been associated with an antiparallel orientation of the weak ferromagnetic component of the canted antiferromagnetic structure with respect to the external magnetic field.[16,17,20] The magnetic structure determined by neutron diffraction below T_t for the V sublattice is $(0,0,G_z)$; the presence of a very weak ferromagnetic component, below the detection threshold of NPD, cannot be excluded. In fact, below 50 K the ferromagnetic component is already detectable by NPD, in a magnetic arrangement defined as $(F_x, 0, G_z)$ for the V^{3+} moments. The abrupt increase of the ferromagnetic component below 50 K accounts for the fact that the magnetization observed in the ZFC susceptibility becomes more negative. Let us point out that the anomalous diamagnetism is associated with an antiparallel orientation of the ferromagnetic component with respect to the magnetic field.

The magnetic moment determined for the V atoms in the magnetic structure resolution, $1.72(4)\mu_B$ at $T = 2.6$ K, suggests that the electronic configuration for the vanadium cations is d^2, which implies a 3+oxidation state. In the VO_6 octahedra, the crystal field splitting of the V $3d$ orbitals de-

termines a $t_{2g}^2 e_g$ electronic configuration for the V^{3+} ions. The octahedral distortion experienced below the crystallographic transition accounts for an additional splitting of the electronic levels into a singlet and a doublet. For a O'-type distortion, with $b/(c\sqrt{2}) < 1$, the ground state is the singlet[16] whereas for the O distortion, $b/(c\sqrt{2}) > 1$, the ground state is the doublet. Therefore, below T_t (O' type) one of the d^2 electrons occupy the singlet and the other is in one of the levels of the doublet.

In the transition from the orthorhombic to the monoclinic structure, a dramatic change takes place in the lattice parameters of the unit cell, although they start to experiment important variations at the magnetic transition T_N, some degrees above T_t. This indicates that the magnetic transition is accompanied by a magnetostrictive effect. Whereas a and c unit-cell parameters increase when cooling across the transition, b notably decreases, which gives rise to the decrease observed in the unit-cell volume. At room temperature the observed O-type distortion is very small, what implies a subtle distortion of the VO_6 octahedra, which in fact could be considered as pseudo-regular octahedra. However, below T_t the O'-type distortion is much stronger, evolving with temperature: a minimum in $b/(c\sqrt{2})$ is reached below 70 K. The two kinds of VO_6 octahedra in the monoclinic phase are alternately compressed along the axial b direction ($V1O_6$) or elongated along the same axial direction ($V2O_6$). Looking at successive a-c planes, across the y direction, we observe that in the $y = 0$ layer, all the V atoms have the long-bond and short-bond V-O pairs along the [10-1] and [101] directions, respectively, whereas in the $y = 1/2$ layer, the long-bond and short-bond pairs are along the [101] and [10-1] directions, respectively (in the orthorhombic phase, the arrangement of the long-bond and short-bond is the same in the $y = 0$ and $y = 1/2$ layers). This arrangement, displayed in Fig. 14, suggests the presence of an orbital ordering, which can be described as follows: the d_{xy} orbital associated with the singlet is occupied at every V position, with the x and y axes taken along the [101] and [10-1] directions. According to Sawada et al. Ref. 33, the two d_{xz} and d_{yz} orbitals, associated with the doublet, with z taken along the [010] direction, would be

occupied depending on the orientation of the long-bond pair. The d_{xz} orbital would be preferentially occupied at the V atoms with a V-O long-bond pair along the x direction, whereas for the d_{yz} orbital the long-bond pair should be in the y direction. So, the occupied orbitals for the V atoms 1, 2, 3, and 4 (defined in Table V) would be, respectively, d_{xy}; d_{yz}, d_{xy}; d_{yz}, d_{xy}; d_{xz}; and d_{xy}; d_{xz}.

With respect to the magnetic structure, the spin arrangement for the V^{3+} ions is given by $(0,0,G_z)$ in the temperature range $50 < T < 136$ K, what implies that the coupling between the V^{3+} ions in the a-c plane is antiferromagnetic, and that the coupling between the a-c planes along the b direction is ferromagnetic. By contrast, in the heavier rare-earth orthovanadates, the magnetic structure is usually given by the basis vector **A**, which implies an antiferromagnetic coupling between the a-c layers along the b direction. On the other hand, in the temperature range $T < 50$ K, the magnetic structure is $(F_x,0,G_z)$ and $(F'_x,0,G'_z)$ for the V^{3+} and Ce^{3+} ions, respectively. For the V^{3+} sublattice, the new ordering implies a reorientation of the moments in the a-c plane. Concerning the ordering of the Ce^{3+} ions, it is very likely due to the V-Ce exchange interaction, as the symmetry of spin arrangement of the Ce^{3+} sublattice is the same as the V^{3+} sublattice. Let us point out that the Ce atoms are arranged in a-c planes, and every Ce layer is between two V layers along the b direction, that present the same spin arrangement.

It is remarkable that the ordering of the rare-earth ions has only been detected in some members of the RVO_3 (Ref. 5) family, in particular those rare-earth cations with strong magnetic moments such as Er^{3+} or Tm^{3+}, and at temperatures lower than 20 K (16 K for $ErVO_3$ and 13 K for $TmVO_3$). In our case, the Ce^{3+} ions order below 50 K, in spite of their relatively weak expected magnetic moment of $2.54\mu_B$.

VI. CONCLUSIONS

The magnetization and specific heat measurements have confirmed that $CeVO_3$ undergoes magnetic ordering below $T_N \approx 136$ K. A negative value in the magnetization is observed in the ZFC susceptibility curve below $T_t \approx 124$ K, indicating the presence of an anomalous diamagnetism. Neutron diffraction measurements have shown that, at T_t, the orthorhombic structure observed at room temperature, space group $Pnma$, becomes monoclinic, space group $P2_1/n$. Across the crystallographic transition there is also a change in the distortion of the VO_6 octahedra: at room temperature the distortion is O type, with $b/(c\sqrt{2}) > 1$ and it changes to O' type with $b/(c\sqrt{2}) < 1$, what implies a change in the orbital ordering.

The magnetic structures are characterized by the propagation vector $\mathbf{k}=0$; immediately below T_N the spin arrangement is given by the basis vector $(0,0,G_z)$, concerning only the vanadium moments. The anomaly observed in the specific heat measurements at around 50 K corresponds to a magnetic transition to another magnetic spin arrangement, also characterized with $\mathbf{k}=0$; on the one hand, a ferromagnetic component appears on the vanadium atoms, which adopt the magnetic structure $(F_x,0,G_z)$, and, on the other hand, the cerium atoms order with a spin arrangement given by $(F'_x,0,G'_z)$. At $T=2.6$ K the magnetic moment for the V^{3+} and Ce^{3+} ions are 1.72(4) μ_B and 0.46(3) μ_B, respectively; the V^{3+} ions present a ferromagnetic component along the a axis of 0.87(6) μ_B, whereas the ferromagnetic components for the Ce^{3+} ions is very weak.

*E-mail address: amunoz@fis.uc3m.es

[1] H.L. Yakel, Acta Crystallogr. **8**, 394 (1955).

[2] F. Bertaut and F. Forrat, J. Phys. Radium **17**, 129 (1956).

[3] S. Geller, Acta Crystallogr. **10**, 243 (1957).

[4] P. Bordet, C. Chaillout, M. Marezio, Q. Huang, A. Santoro, S-W. Cheong, H. Takagi, C. S. Oglesby, and B. Batlogg, J. Solid State Chem. **106**, 253 (1993).

[5] V.G. Zubkov, G.V. Bazuev, and G.P. Shveikin, Sov. Phys. Solid State **18**, 1165 (1976).

[6] K. Hazuki, Y. Hideki, and U. Yutaka, J. Phys. Soc. Jpn. **63**, 2857 (1994).

[7] G.V. Bazuev, I.I. Matveenko, and G.P. Shveikin, Sov. Phys. Solid State **16**, 155 (1974).

[8] T. Sakai, G. Adachi, J. Shiokawa, and T. Shin-ike, Mater. Res. Bull. **11**, 1295 (1976).

[9] D. B. Rogers, A. Ferretti, D. H. Ridgley, R. J. Arnott, and J.B. Goodenough, J. Appl. Phys. **37**, 1431 (1966).

[10] P. Dougier and P. Hagenmuller, J. Solid State Chem. **15**, 158 (1975).

[11] Y. Kimishima, M. Takahashi, K. Iga, K. Okada, and Y. Ichiyanagi, Physica B **194-196**, 211 (1994).

[12] Y. Kimishima, M. Takahashi, K. Okada, H. Ishikawa, and Y. Ichiyanagi, J. Magn. Magn. Mater. **140-144**, 1185 (1995).

[13] M. Onoda and H. Nagasawa, Solid State Commun. **99**, 487 (1996).

[14] Y. Kimishima, Y. Ichiyanagi, K. Shimizu, and T. Mizuno, J. Magn. Magn. Mater. **210**, 244 (2000).

[15] A. Muñoz, J.A. Alonso, M.T. Casais, M.J. Martínez-Lope, J.L. Martínez, and M.T. Fernández-Díaz, J. Mater. Chem. **13**, 1234 (2003).

[16] H.C. Nguyen and J.B. Goodenough, Phys. Rev. B **52**, 324 (1995).

[17] H.C. Nguyen and J.B. Goodenough, J. Solid State Chem. **119**, 24 (1995).

[18] Y. Ren, T.T.M. Palstra, D.I. Khomskii, A.A. Nugroho, A.A. Menovsky, and G.A. Sawatzky, Nature (London) **396**, 441 (1998).

[19] Y. Ren, T.T.M. Palstra, D.I. Khomskii, A.A. Nugroho, A.A. Menovsky, and G.A. Sawatzky, Phys. Rev. B **62**, 6577 (2000).

[20] J.B. Goodenough and H.C. Nguyen, C. R. Acad. Sci., Ser. IIb: Mec., Phys., Chim., Astron. **319**, 1285 (1994).

[21] G.R. Blake, T.T.M. Palstra, Y. Ren, A.A. Nugroho, and A.A. Menovsky, Phys. Rev. Lett. **87**, 245501 (2001).

[22] A. S. Borukhovich, G.V. Bazuev, and G.P. Shveikin, Sov. Phys. Solid State **15**, 2203 (1973).

[23] A. S. Borukhovich, G.V. Bazuev and G.P. Shveikin, Sov. Phys. Solid State **16**, 286 (1974).

[24] A. S. Borukhovich and G.V. Bazuev, Sov. Phys. Solid State **16**, 273 (1974).

[25] A. S. Borukhovich, V.G. Zubkov, and G.V. Bazuev, Sov. Phys. Solid State **20**, 1049 (1978).

[26] H.M. Rietveld, J. Appl. Crystallogr. **2**, 65 (1969).

[27] J. Rodríguez-Carvajal, Physica B **192**, 55 (1993).

[28] F. Millange, S. de Brion, and G. Chouteau, Phys. Rev. B **62**, 5619 (2000).

[29] N.J. Poirot, Ch. Allanon, P. Odier, P. Simon, J.M. Bassat, and J.P. Loup, J. Solid State Chem. **138**, 260 (1998).

[30] S. Nagata, H. Sasaki, K. Suzuki, J. Kiuchi, and N. Wada, J. Phys. Chem. Solids **62**, 1123 (2001).

[31] A. Muñoz, J.A. Alonso, M.J. Martínez-Lope, J.L. García-Muñoz, and M.T. Fernández-Díaz, J. Phys.: Condens. Matter **12**, 1361 (2000).

[32] In a previous trial magnetic refinement in the temperature range $50 < T < 136$ K, the solution $(G_x, 0, 0)$ also yields to a good agreement with the experimental data. However, below 50 K, on considering the solution $(G_x, 0, F_z)$ and $(G'_x, 0, F'_z)$ for the V^{3+} and Ce^{3+} ions, respectively (they belong to the same irreducible representation), the agreement with the experimental data is significantly worse than for $(F_x, 0, G_z)$ and $(F'_x, 0, G'_z)$ for the V^{3+} and Ce^{3+} ions. It seems reasonable that the z component of the moment is given by G_z in all the ordering region, thus this solution has been selected to describe the magnetic structure.

[33] H. Sawada, N. Hamada, K. Terakura, and T. Asada, Phys. Rev. B **53**, 12 742 (1996).